World Scientific
www.worldscientific.com

STATIC AND SPONTANEOUS ELECTROWETTING

LESLIE Y. YEO* and HSUEH-CHIA CHANG

*Department of Chemical and Biomolecular Engineering,
University of Notre Dame, Notre Dame, IN 46556, USA*

There has been recent renewed interest in electrocapillary and electrowetting phenomena given its potential for microfluidic actuation and manipulation. Different approaches, in which a variety of electrode configurations have been adopted, however, have dominated the developments in this field. These different approaches have given rise to rich and varied behavior, which has often led to some overlap and confusion in the literature. In this article, we delineate the different observations and elucidate the relationship between these phenomena by re-stressing classical concepts and examining their limitations. Particular emphasis is placed on the distinction between static and spontaneous electrowetting. In the former, a static change in the liquid–solid macroscopic contact angle results when a dielectric film-coated planar plate electrode is employed. In the latter, a spontaneous thin front-running electrowetting film is pulled out ahead of the macroscopic drop with the use of planar parallel line electrodes. This dynamically evolving electrowetting film advances much faster than the macroscopic drop itself and behaves in a self-similar manner analogous to gravity spreading films.

Keywords: Electrowetting; electrocapillary phenomena; interfacial tension; electric fields; thin films.

1. Introduction

Electrocapillary phenomena dates back to the early observations of Lippmann[1] who noted variations in interfacial tension as an electric potential is applied. The Lippmann electrometer is shown in Fig. 1(a) demonstrating the principle of electrocapillarity. As the potential applied to the mercury is increased, the meniscus position of the polarized mercury/electrolyte interface (within the small tube at the bottom of the long column) is altered. By adjusting the height of the mercury reservoir h such that the meniscus is returned to its original position, the change in the interfacial tension with applied potential can be quantified, as illustrated in Fig. 1(b). The maximum in the electrocapillary curve in Fig. 1(b) occurs as the isopotential point is achieved, i.e. when the counterions in the electrolyte exactly

*Present address: Department of Mechanical Engineering, Monash University, Clayton, VIC 3800, Australia.
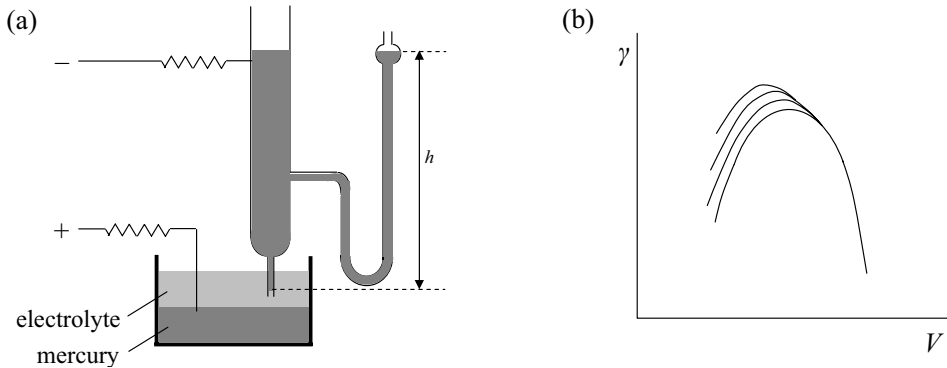
(a)

(b)

Fig. 1.   (a) The Lippmann capillary electrometer. (b) Electrocapillary curves for different electrolytes. The maximum in the curves is the isopotential point or the potential of zero charge.

balance the charge on the surface such that the net surface charge and electrokinetic potential are zero, resulting in the collapse of the Debye double layer (complete screening limit). The change in the mercury/electrolyte interfacial tension γ with applied potential V is then described by the classical Lippmann equation:

$$\left(\frac{\partial \gamma}{\partial V}\right)_{T,P,\mu} = -\sigma \,, \tag{1}$$

where T is the temperature, P the pressure, and μ the chemical potential. The surface charge density σ can be expressed as

$$\sigma = \frac{C}{A}V = \frac{\epsilon_o \epsilon_l}{d}V \,, \tag{2}$$

where C is the capacitance of the double layer with cross-sectional area A and separation d, ϵ_l is the relative permittivity of the liquid and ϵ_o is the permittivity of vacuum, respectively. It then follows from Eqs. (1) and (2) that

$$\Delta \gamma = -\frac{\epsilon_o \epsilon_l}{2d}V^2 \,. \tag{3}$$

The double layer is on the electrolyte side of the mercury/electrolyte interface and, since both the mercury and electrolyte are conducting media, most of the voltage drop V is across this double layer.

The Lippmann equation is the fundamental basis for electrowetting, which attempts to control the wettability of a liquid precisely and rapidly with electrical fields in the absence of mechanically moving parts. Recent interest in such efforts have been driven by the need for fluid handling and actuation mechanisms in microfluidic devices.[2] Bockris and Reddy[3] nevertheless propose a fundamental distinction between the classical Lippmann *electrocapillary phenomena* and *electrowetting*. In classical electrocapillarity, described in the previous paragraph, the applied electric field energetically favors a change in the solid or liquid metal–electrolyte interfacial tension, i.e. there is an increase in the interfacial contact between the metal

and the electrolyte, as shown in Fig. 2(a).[4,5] Electrowetting, at least for static contact angles without spontaneous spreading, has traditionally been concerned with the change in the macroscopic liquid–solid wetting angle θ subtended when the vapor/liquid, liquid and solid phases coincide at the three-phase contact line. Nevertheless, the force balance at the contact line necessarily involves the vapor/liquid–liquid interfacial tension γ. As such, the electrocapillary phenomena can be related to static electrowetting. Substituting Young's equation, which represents a balance of tangential forces at the vapor–liquid–solid contact line,

$$\gamma_{\mathrm{LV}} \cos \theta = \gamma_{\mathrm{SV}} - \gamma_{\mathrm{SL}} \,, \tag{4}$$

where γ_{LV}, γ_{SV} and γ_{SL} are the vapor–liquid, vapor–solid and liquid–solid interfacial tensions, respectively, into Eq. (1) with $\gamma = \gamma_{\mathrm{SL}}$ such that

$$\frac{\mathrm{d}(\cos \theta)}{V \, \mathrm{d}V} = \frac{C}{\gamma_{\mathrm{LV}}} \,. \tag{5}$$

The equivalent Lippmann condition for electrowetting then reads

$$\cos \theta = \cos \theta_0 + \frac{\epsilon_o \epsilon_l}{2 d \gamma_{\mathrm{LV}}} V^2 \,. \tag{6}$$

In the above, θ_0 is the contact angle in the absence of an electric field and $\epsilon = \epsilon_o \epsilon_l$ is the electrolyte permittivity. $\epsilon V^2 / 2d$ is hence the electrocapillary force per unit length (linear force density) in the solid plane along the contact line, assuming that the electrode configuration is such that the voltage drop V is mostly across a dielectric film on the plane. The electric field has changed the vapor-liquid surface force and hence altered the static contact angle when all three surface forces balance. Electrowetting, therefore, involves a slightly different configuration in which the metal electrode is coated with an insulating dielectric, as shown in Figs. 2(b) and 2(c). These electrode configurations are known in the literature as electrowetting on dielectric (EWOD) or electrowetting on insulator-coated electrodes (EICE) schemes. We note therefore that although Lee and Kim[5] have termed their setup, depicted in Fig. 2(b) as *continuous electrowetting*, it is strictly speaking, more akin to *classical electrocapillarity* because it involves a change in the liquid metal–electrolyte contact angle.

However, by utilizing a parallel line electrode configuration as shown in Fig. 2(d), in place of the typical dielectric film-coated electrode (EWOD/EICE) configurations shown in Figs. 2(b) and 2(c), a spontaneous electrowetting film is produced instead of a static change in the macroscopic contact angle. Jones[6] has previously attempted to distinguish between the two phenomena by defining the former [Fig. 2(d)] and the height-of-rise experiments [Fig. 2(e)] as dielectrophoretic (DEP) actuation and the latter [Figs. 2(b) and (c)] as electrowetting. DEP force is a normal interfacial force due to field-induced interfacial polarization.[7,8] It has, in fact, the same physical origin as the electrocapillary phenomenon, although a very different electrode geometry is required for spontaneous electrowetting. In addition, the Lippmann condition given by Eq. (3) is generally no longer valid.
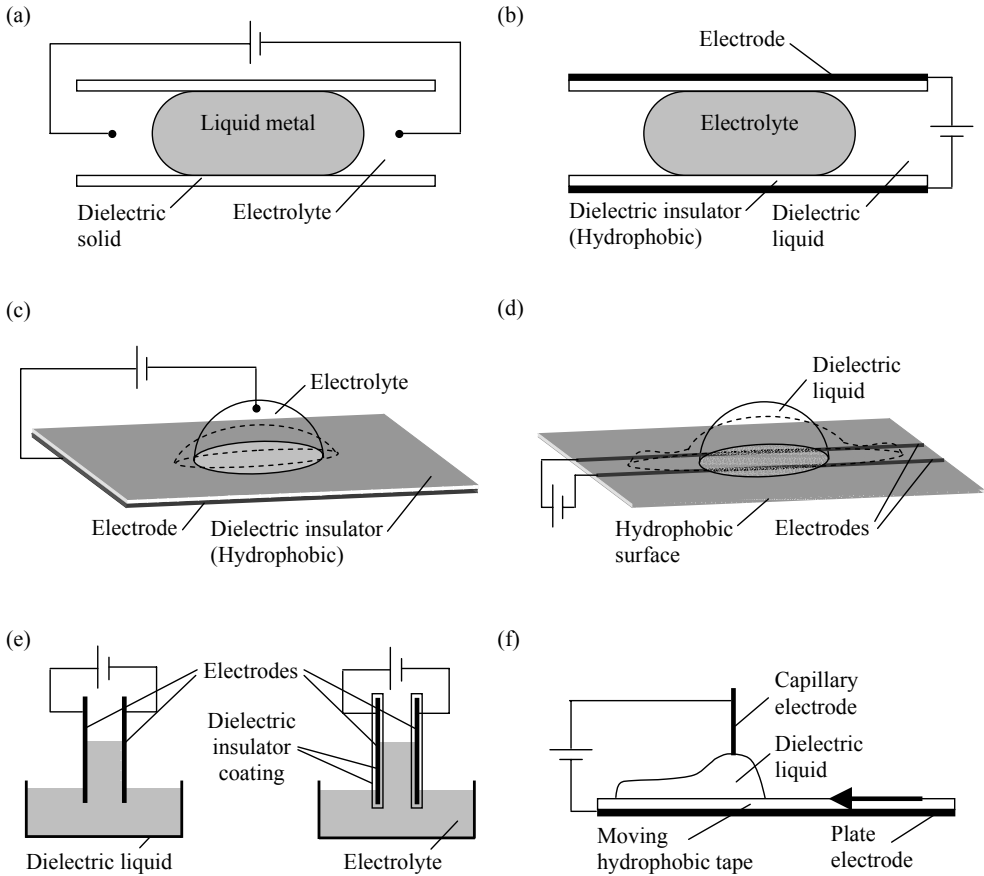
(a)

Liquid metal

Dielectric solid   Electrolyte

(b)

Electrode

Electrolyte

Dielectric insulator (Hydrophobic)   Dielectric liquid

(c)

Electrolyte

Electrode   Dielectric insulator (Hydrophobic)

(d)

Dielectric liquid

Hydrophobic surface   Electrodes

(e)

Electrodes

Dielectric insulator coating

Dielectric liquid   Electrolyte

(f)

Capillary electrode

Dielectric liquid

Moving hydrophobic tape   Plate electrode

Fig. 2.   Typical schematic electrode configurations used in electrocapillary and electrowetting experiments. (a) Electrode configuration demonstrating electrocapillarity, which involves a static change in the liquid metal–electrolyte contact angle. (b) Dielectric film-coated top and bottom plate electrodes giving rise to static changes in the liquid–solid contact angle. (c) Dielectric film-coated planar plate electrode giving rise to static changes in the liquid–solid contact angle. (d) Planar parallel line electrode configuration giving rise to spontaneous and dynamically advancing thin electrowetting films. (e) Classical height-of-rise experiments (the diagram on the left shows the rise of an insulating dielectric liquid whereas the diagram on the right shows a modified setup to allow for the rise of an electrolyte using electrodes coated with a dielectric layer). (f) Modification of the dielectric film-coated planar plate electrode configuration in (c) to allow for moving contact lines.

The normal DEP force density on a liquid body experiencing a purely normal field E_n can be converted to a Maxwell pressure

$$p_M = \frac{\epsilon_o \epsilon_l}{2} E_n^2.$$ (7)

If both the liquid and ambient phases are conducting and if the field is normal to the double layer of thickness d that exists at the interface, $E_n = V/d$ and hence

the Maxwell pressure given by Eq. (7) becomes $\epsilon V^2/2d^2$, where $\epsilon = \epsilon_o \epsilon_l$ is the electrolyte permittivity. On a planar interface, this pressure would contribute to the linear force density $\epsilon V^2/2d$ corresponding to the Lippmann conditions in Eqs. (3) and (6). Such conditions correspond to the configurations given by Figs. 2(a) and 2(b) in which spontaneous electrowetting does not occur.

As discussed earlier, a dielectric film thickness d can replace the double layer, such as given by the configuration in Fig. 2(c). This case will be shown in Sec. 2.2 to also produce the Lippmann condition. We will show subsequently that only a static change in the macroscopic contact angle arises; spontaneous electrowetting cannot be achieved with this configuration. Moreover, the liquid above the dielectric film must be conducting and the electric field must be directed normal to the dielectric film. There is no surface tension associated with a solid dielectric film, however. The contact line lying on this dielectric film will thus experience an electrocapillary effect due to the Maxwell pressure across the dielectric film and hence the dielectric Maxwell pressure becomes an electrocapillary effect at the contact line.

Nevertheless, there are very few examples where the interface is between two conducting liquids such that the field is always normal to the interface and that most of the voltage drop V is across the double layer or across the dielectric film at the interface. More often, the interfacial Maxwell pressure should generally involve contributions from both the normal and tangential electric fields such that

$$p_M = \frac{\epsilon_o \epsilon_l}{2}(E_n^2 - E_t^2),\tag{8}$$

when the permittivity of one phase is negligible.[9] The tangential field E_t cannot be described by V/d and hence the connection between electrocapillarity and interfacial polarization and force becomes tenuous. The field components need to be solved explicitly for an arbitrary interfacial shape and cannot be approximated in the way that the normal field is approximated by V/d. Even if the interfacial field and Maxwell pressure can be resolved, the bulk pressure gradient that drives the flow in spontaneous electrowetting [Fig. 2(d)] still needs to be determined from the hydrodynamic equations of motion. This is difficult to do in general, especially if a generic description of the dynamic contact angle condition is to be derived to replace its static counterpart in Eq. (6). The hydrodynamic problem, unfortunately, is simply too complex to solve in general, and is complicated further by the different drop and electrode geometries (some of which are shown in Fig. 2) that can produce the requisite pressure gradient.

In spontaneous thin front-running electrowetting films of highly wetting fluids, the tangential Maxwell pressure gradient at the interface is exactly the bulk Maxwell pressure gradient since there is no normal pressure gradient in the thin film or long-wave limit. The hydrodynamics therefore becomes simplified and Yeo and Chang[10] were able to derive a generic dynamic contact angle condition for electrowetting. These complex relationships between static and spontaneous (dynamic) electrowetting will be reviewed here. The theory introduced here applies

for both dc and ac electric fields. However, with ac fields, charge relaxation becomes important, especially when electrolyte is used and the charging/discharging capacitance effects of the double layer becomes signficant. Double-layer polarization can overwhelm dielectric polarization and, depending on the applied frequency of the ac field, can periodically change the interfacial field from a predominantly normal field to a screened tangential field. Such charge relaxation and screening phenomena produce frequency-dependence in the electrowetting dynamics with ac fields. These effects will not be analyzed here; any dynamic capacitance effects are assumed to be negligible. In this theory, there is therefore no distinction between dc and ac fields. The interfacial field is simply stipulated to be either tangentially or normally dominant.

The most curious distinction between static and spontaneous electrowetting, however, is the absence of a bulk pressure gradient in the former to drive a wetting flow. For this to occur, the dependence of the interfacial tension on the electric field described by the Lippmann equation in Eq. (3) or a more generalized version of it must be confined to the three-phase contact line. (More precisely, it is the interfacial tension gradient that suffers this confinement; otherwise, electro-Marangoni effects could still arise to drive a bulk flow.) At the contact line, the surface forces can compensate the electrocapillary force, as given by Eq. (6), such that no pressure gradient exists in the bulk. The reason why the electrocapillary force is confined to the contact line cannot be argued by the simple physical considerations given above and will be the focus of this review. However, it is quite clear that for both static and spontaneous electrowetting, the Lippmann condition in Eq. (3) is invalid when a generalized Maxwell pressure involving both normal and tangential components of the electric field, as given by Eq. (8), is involved.

A further distinction should be made between these spontaneous electrowetting films and *dynamic electrowetting*, which has important applications in electro-assist coating technology. The term "dynamic electrowetting" was used by Schneemilch *et al.*[11] and Blake *et al.*[12] to describe the process in which the dielectric film coating in the EWOD/EICE configurations is conveyed over a grounded coating roller, as shown in Fig. 2(f). With this geometry, it should be noted that the electric field does not contribute to the forces at the contact angle of the front-running film dragged out by the moving layer since the field is weak at this point. This is because the EWOD/EICE electrode configuration, which remains much the same in this setup except for the moving dielectric layer, cannot give rise to spontaneous electrowetting, as will be shown subsequently. The contact angle here evolves dynamically, solely due to the action of a moving contact line as a result of the shear imposed by the conveying layer.

2. Static Electrowetting

2.1. *Experimental observations and deviations from the Lippmann condition*

The EWOD/EICE configuration shown in Figs. 2(b) and 2(c) consists of an insulating layer, typically a dielectric material (e.g. polymer substrate) several microns to millimeters in thickness to eliminate electrolysis, deposited onto a conducting plate. In cases where the insulating layer is not hydrophobic (e.g. parylene), a very thin hydrophobic layer such as a fluoropolymer of order nanometers in thickness, is coated onto the insulator. When an ac or dc electric field is applied across the plate and a line electrode brought into contact with the liquid drop, a large change in the macroscopic solid–liquid contact angle of the drop is observed. However, the observed change in the contact angle is static and proportional to the square of the applied voltage. As such, there have been numerous efforts to correlate the observed change in the contact angle to the Lippmann condition in Eq. (6).[13,14]

Below a critical applied voltage, the experimental contact angle measurements can be universally described by the Lippmann condition. Above this limiting value, however, contact line saturation occurs before complete wetting is achieved. Upon saturation, the results begin to deviate from the behavior described by the Lippmann condition. In addition, near the saturation point, contact angle hysteresis is observed: the receding contact angle upon decreasing the voltage is observed to be smaller than the advancing contact angle at increasing voltage. It should be noted that this hysteresis effect is distinct from the usual contact angle hysteresis that occurs in drops on inclined planes, where the receding contact angle is always greater than the advancing contact angle.

These saturation effects have been attributed to several factors. One reason for saturation is due to dielectric breakdown of the atmosphere in the contact line region,[15] although this effect is observed to be more pronounced when dc fields are employed. This is supported by the results of Vallet *et al.*[15] who showed that the saturation threshold voltage at which the measurements begin to deviate from the Lippmann condition coincides closely with the ionization voltage. When the atmosphere ionizes, the ambient phase no longer acts as an insulator wherein the charges that accumulate at the contact line exert an outwardly directed Maxwell force which gives rise to the spreading. As a result, the leakage of charges into the ambient phase weakens this Maxwell force, thus suppressing the electrowetting behavior.[15]

When the ambient medium is water surrounding a dielectric liquid drop, contact line saturation has been suggested to arise due to charge leakage from the aqueous phase into the insulating polymer layer at high field intensities.[13,16] Janocha *et al.*[13] also suggest that it is the delayed release of the leaked charges from the polymer surface back into the aqueous phase when the voltage is decreased that is responsible for the contact angle hysteresis observed.

Below the saturation threshold voltage, the deviation of the results from the theoretical predictions has also been attributed to double-layer effects. Quinn *et al.*[17] proposed that specific ion adsorption at the interface between the aqueous drop and the insulating polymer surface is responsible for the asymmetric deviation of the contact angle behavior from theory. Deviations occurred at voltages significantly lower than the saturation threshold voltage only when a positive potential was applied. They therefore suggest that OH^- ions in the aqueous solution specifically adsorp onto the polymer surface when positive voltage is applied, thus increasing the cation concentration in the aqueous drop phase and hence the charge accumulation at the contact line which gives rise to the spreading. At a particular voltage, however, saturation occurs and further ion adsorption ceases, therefore reducing the charging efficiency and hence leading to the deviation of the results from the Lippmann condition. On the other hand, when negative potentials are applied, the OH^- ions are repelled from the polymer surface and hence the abovementioned effects are not observed. Their postulation is further supported by experimental results that demonstrate the deviation to be sensitive to ionic concentration.

2.2. *Theoretical framework*

Several theories for static electrowetting have been proposed to describe the static change in the macroscopic liquid–solid contact angle due to the influence of the electric field. Using variational theory, Digilov[18] proposed that the electrowetting effect is due solely to line tension rather than surface tension effects, the change in the contact angle arising due to the decrease in line tension as a result of charge redistribution along the contact line (i.e. the excess free energy at the contact line). Nevertheless, this has not been widely accepted since there have been no conclusive evidence to show that the contact angle is dependent on the drop size, which would have been observed if the theory is true.[19] Other theoretical descriptions have been proposed based on molecular kinetic,[14,20] electromechanic[21] and static[22] analyses. The electromechanic approach accounts for the equilibrium free energy of Coulombic interactions of a charged drop at the contact line, whereas in the static approach, equilibrium drop shapes have been generated by a local dominant balance between the electrostatic and capillary forces at the contact line region. The molecular kinetic approach, in contrast, considers the viscous dissipation energy that arises due to the liquid and solid molecular interactions at the contact line which provides a mechanism for slip between the liquid and the solid surface, thereby removing the difficulties associated with the stress singularity at the contact line.[23,24]

Both Vallet *et al.*[15] and Kang[25] have modeled static electrowetting of a drop on a dielectric film-coated planar plate configuration [Fig. 2(c)] by considering an infinite planar wedge analysis in the three-phase contact line region, as shown in Fig. 3. As the electrode is in contact with the drop phase, represented by the wedge, it is assumed to be a perfect conductor at constant potential and surrounded by a perfectly insulating ambient medium. Since the dielectric permittivity of the

polymer layer (with thickness d) is low, the permittivities of the ambient medium and the substrate are assumed to be equal. In the absence of any free space charge, the electrostatic potential in the ambient medium ϕ then obeys the Laplace equation:

$$\nabla^2 \phi = 0\,, \tag{9}$$

subject to the constant potential interface boundary conditions,

$$\phi = 0 \quad \text{on} \quad \Gamma \quad \text{and} \quad \Gamma_d\,, \tag{10}$$

and

$$\phi = V \quad \text{on} \quad \Gamma_s\,, \tag{11}$$

where Γ, Γ_d and Γ_s denote the interfaces between the drop and the ambient phase, the drop and the dielectric layer, and, the dielectric layer and solid interfaces, respectively. The tangential field here is assumed to be negligible, i.e. $E_t = 0$. Eqs. (9)–(11) can be solved using the Schwarz–Christoffel transformation[15,25]:

$$Z = \int_{i\pi}^{w} (e^{w'} + 1)^\alpha dw' + i\pi\,, \tag{12}$$

where $Z = x + iy$ ($i = \sqrt{-1}$) and $w = u + iv$ are the complex coordinates of the transformed plane with u and v scaled by d/π and V/π, respectively. $\alpha = p/q = 1 - \theta/\pi$, where p and q are positive integers and θ is the contact angle of the drop. Vallet *et al.*[15] then obtained the following expression for the normal field at the interface between the drop and the ambient phase E_n:

$$E_n = \frac{V}{d} \frac{1}{(e^u - 1)^\alpha}\,. \tag{13}$$

Adopting a cylindrical coordinate system $(r, \theta', 0)$, where r is the radial distance from the wedge tip, defined from Eq. (12) by[25]

$$r = \frac{d}{\pi} \int_0^u |e^{u'} - 1|^\alpha du'\,, \tag{14}$$

$r = 0$ being defined at the wedge tip, we note that for small contact angles, i.e. as $\theta \to 0$, E_n is singular and blows up as

$$E_n \sim \frac{1}{|r|^{1/2}}\,. \tag{15}$$

In fact, E_n is always weakly singular for all $\theta < \pi$, the singularity being most significant the smaller the contact angle. Figure 3 schematically shows how this normal field blows up at the wedge tip where the three-phase contact line is located. We observe, however, that this weakly singular field only blows up in a very confined region with a length scale of order d. Since the Maxwell pressure $p_M \sim E_n^2$, the Maxwell pressure gradient that arises as a result is localized in this confined region at the contact line and cannot give rise to any bulk flow below the advancing contact angle.
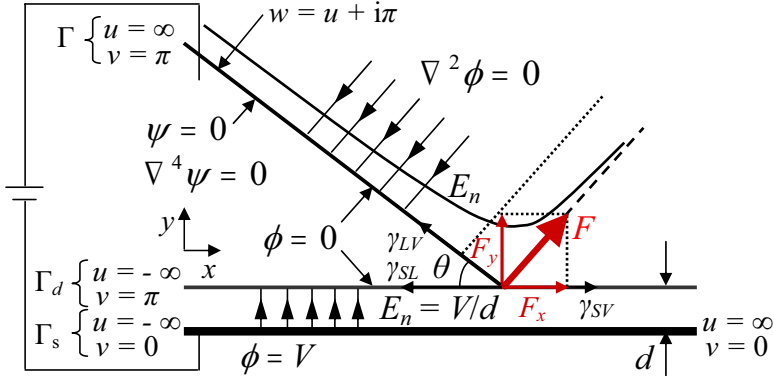
Fig. 3.   Wedge analysis representing the drop geometry in the contact line region. *Black arrows* indicate the direction of the field and *light bold arrows* indicate the resultant point force and its components at the contact line. The curve depicts the charge density or the normal field intensity along the drop interface which is singular at the tip or the three-phase contact line for all $\theta < \pi$.

The absence of bulk flow into the contact line region can also be observed by considering the hydrodynamics in this region. Rotating the wedge in Fig. 3 in the cylindrical coordinate system defined above such that it is symmetric about $\theta' = \pi$, the stream function ψ satisfies the biharmonic equation

$$\nabla^4 \psi = 0 \,, \tag{16}$$

with the boundary condition

$$\psi = 0 \,, \tag{17}$$

on Γ and Γ_d, i.e. on $\theta' = \pm (\pi - \theta/2)$, for steady viscous flow of an incompressible Newtonian fluid. For

$$u_r = \frac{1}{r}\frac{\partial \psi}{\partial \theta'}, \qquad \text{and} \qquad u_{\theta'} = -\frac{\partial \psi}{\partial r} \,, \tag{18}$$

to remain bounded as $r \to 0$ and for the boundary condition given by Eq. (17) to hold, the pressure p can be shown from a harmonic expansion of the biharmonic equation to read[16]

$$p \sim \tilde{A} + \tilde{B}r + \sum_{m=2}^{\infty} (\tilde{C}r^{m-2} + \tilde{D}r^m) \,, \tag{19}$$

where $\tilde{A}$, $\tilde{B}$, $\tilde{C}$ and $\tilde{D}$ are arbitrary constants. At the wedge tip as $r \to 0$, the hydrodynamic pressure is never singular since $m \geq 2$. We therefore note from a normal stress jump across the isopotential interface where $E_t = 0$,

$$p = \gamma\kappa + p_M = \gamma\kappa + \frac{\epsilon}{2}E_n^2, \tag{20}$$

where κ is the mean interfacial curvature and ϵ is the permittivity of the dielectric layer, that the behavior of the hydrodynamic pressure given by Eq. (19) as $r \to 0$ is

incompatible with the interfacial normal stress jump condition involving a singular Maxwell stress $\epsilon E_n^2/2$, in which E_n blows up in the manner stipulated by Eq. (15).

To carry this point further, the localized region in which the Maxwell pressure gradient is significant is too small to be resolved in the continuum limit. In order to obtain the net Maxwell force F, coarse graining or integration to average the Maxwell stress is then required to obtain a finite pressure or force density[25]:

$$F = \frac{\epsilon}{2} \int_\Gamma E_n^2 \mathrm{d}r \,. \tag{21}$$

It then follows from Eqs. (13) and (14) that

$$F = \frac{\epsilon V^2}{2\pi d} \int_0^\infty \frac{\mathrm{d}u}{|e^u - 1|^\alpha} \,, \tag{22}$$

which Kang[25] shows to result in a net point force F at the contact line:

$$F = \frac{\epsilon V^2}{2d} \operatorname{cosec} \theta \,, \tag{23}$$

which can be further decomposed into its horizontal and vertical components

$$F_x = \frac{\epsilon V^2}{2d} \qquad \text{and} \qquad F_y = \frac{\epsilon V^2}{2d} \cot \theta \,, \tag{24}$$

respectively. Due to the planar geometry, F_x is actually the force per unit length of the contact line. We note that upon balancing the surface forces at the contact line, the Lippmann condition in Eq. (6) is recovered, the Maxwell pressure correction in Eq. (24) accounting for the static change in the macroscopic contact angle. Since the point Maxwell force balances the surface forces exactly, there is no net force and hence no bulk liquid flow into the contact line region. We have omitted any Maxwell pressure gradients away from the contact line. Thus, only a static change in the macroscopic contact angle results; there is no spontaneous electrowetting film produced in the absence of any bulk fluid motion. The arguments above therefore show that spontaneous electrowetting films cannot be produced using the dielectric film coated planar plate electrode (EWOD/EICE) configuration in Fig. 2(c). In the next section, we will discuss why a spontaneous electrowetting film is produced using a planar parallel line electrode configuration in Fig. 2(d).

3. Spontaneous Electrowetting

Spontaneous electrowetting films, in which a thin liquid film is pulled out ahead of the macroscopic spreading drop due to an applied electric field, were first observed by Jones *et al.*[27] and Ahmed *et al.*[28] using the parallel line electrode configuration shown in Fig. 2(d). This thin electrowetting film advances much faster than the macroscopic spreading drop itself and should not be confused with the molecular precursor films associated with perfectly wetting or partially wetting liquids that wet the solid substrate due to molecular forces at the contact line.[29] The

molecular precursor film is microscopic, several angstroms in thickness, whereas the electrowetting film is macroscopic, with thicknesses of several microns.

Jones *et al.*[27] attribute these spontaneous electrowetting films to dielectrophoretic (DEP) actuation of high permittivity, polar dielectric liquids, suggesting that the spontaneous electrowetting film produced is due to the same mechanism that results in the bulk upward motion of the liquid between two vertical electrodes in the classical height-of-rise experiments.[6] However, whilst the height-of-rise do exhibit strong frequency dependence when an ac field is applied that is characteristic and indicative of the DEP mechanism, there has yet to be systematic observations documented to suggest that spontaneous electrowetting films show the same dependence on frequency. Moreover, the derivation of Jones' model involves a macroscopic ponderomotive force that applies on the entire bulk of the liquid. Solution of the Stokes equation to resolve the hydrodynamics was never carried out. This ponderomotive force therefore cannot be localized to indicate where it acts on the liquid.[25] In addition, the purely electrostatic model falls short of providing any hydrodynamic mechanism that can capture the dynamic contact angle or the evolution dynamics of the electrowetting film.

Yeo and Chang,[10] on the other hand, have derived a model based on the coupling between the electrodynamics and hydrodynamics that results in the generation and propagation of a spontaneous electrowetting film ahead of the macroscopic spreading drop. This spontaneous electrowetting film is shown to arise due to a bulk Maxwell pressure gradient in the contact line region. In contrast to the singular Maxwell stress at the contact line in static electrowetting, as discussed in Sec. 2.2, the Maxwell stress that arises here is not singular nor is it confined to a localized region. As a result, this macroscopic Maxwell pressure gradient produces a negative capillary pressure that induces bulk liquid to flow into the contact line region thus spontaneously pushing out a thin electrowetting film ahead of the macroscopic drop.

We proceed to present relevant scaling arguments and details of the model[10] to capture the spreading dynamics of a high permittivity dielectric liquid drop ($\epsilon_l \gg \epsilon_g$, where ϵ_g is the permittivity of the ambient vapor phase). The hydrodynamics is described by the equations governing mass and momentum conservation for an incompressible fluid in the long-wave limit in which a slender drop is assumed (see Fig. 4), i.e. the characteristic drop height H is small compared to the characteristic streamwise and transverse drop length scales L such that $\varepsilon \equiv H/L \ll 1$:

$$\frac{\partial u}{\partial x} + \frac{\partial v}{\partial y} = 0 \,; \tag{25}$$

$$\frac{\partial p}{\partial x} = \mu \frac{\partial^2 u}{\partial z^2} \,. \tag{26}$$

Here, u and v are the velocities in the streamwise (x-coordinate) and vertical (z-coordinate) directions, respectively; p and μ, on the other hand, are the fluid pressure and viscosity, respectively. The velocity in the transverse (y-coordinate) direction is negligible since the side contact lines of the electrowetting film is assumed
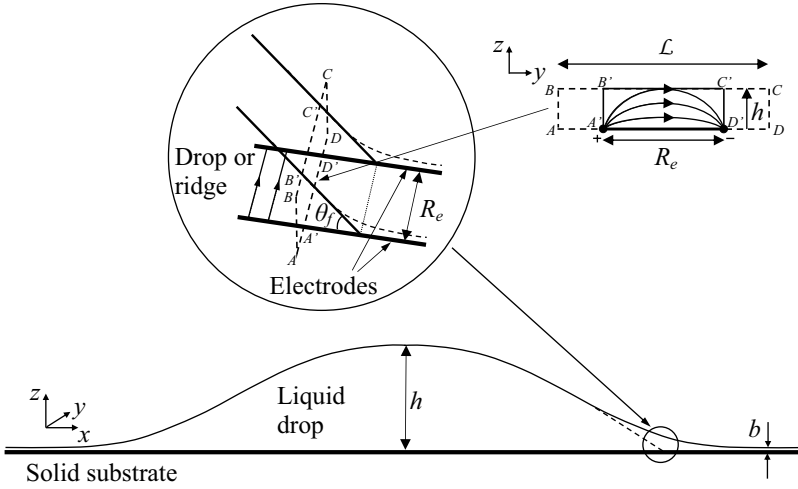
Fig. 4. Schematic depiction of the macroscopic drop. The inset shows a magnification of the contact line region in which the drop or the capillary ridge of the electrowetting film resembles a wedge-like geometry. A cross-section $ABCD$ of this wedge and the transverse field lines arising due to the line electrodes, which resemble two point charges in this plane, are also shown.

to be stationary. Furthermore, the electrowetting film is assumed to be sufficiently flat such that the film thickness h does not have any y-dependence.

The usual no-slip boundary condition applies on the solid substrate Γ_s where $z = 0$:

$$u = v = 0 \qquad \text{on} \quad \Gamma_s. \tag{27}$$

At the air–drop interface Γ where $z = h$, the following tangential stress balance, normal stress jump and kinematic boundary conditions apply:

$$\frac{\partial u}{\partial z} = 0 \qquad \text{on} \quad \Gamma, \tag{28}$$

$$p = \gamma \frac{\partial^2 h}{\partial x^2} + p_M \qquad \text{on} \quad \Gamma, \tag{29}$$

and

$$\frac{\partial h}{\partial t} + \frac{\partial}{\partial x}(h\bar{u}) = 0 \qquad \text{on} \quad \Gamma, \tag{30}$$

where $\bar{u}$ is the cross-sectional mean velocity across the film height, and E_{t_l} is the tangential component of the liquid phase electric field. We note from the interfacial jump conditions for the electric field in the absence of free space charge,

$$\epsilon_l E_{n_l} = \epsilon_g E_{n_g} \qquad \text{on} \quad \Gamma, \tag{31}$$

and

$$E_{t_g} = E_{t_l} \qquad \text{on} \quad \Gamma, \tag{32}$$

that the liquid phase normal field component E_{n_l} as well as the vapor phase normal and tangential field components, E_{n_g} and E_{t_g}, respectively, are negligible in the limit $\epsilon_l \gg \epsilon_g$. Therefore, only E_{t_l} appears in Eq. (29), which provides the coupling between the hydrodynamic and electrodynamic mechanisms.

To obtain E_{t_l}, the following electrodynamic model was adopted, noting that the transverse y-dependence, which was absent in the hydrodynamic model due to the flatness of the electrowetting film, becomes dominant due to the polarity of the electrodes. The geometry of the system is shown by the cross-section $ABCD$ in the y–z plane in the inset of Fig. 4. In this plane, the two line electrodes can be represented by two point charges on the solid substrate Γ_s. Since the free space charge due to capacitance storage of charges in the double layer is assumed to be negligible, the electrostatic potential in the liquid phase ϕ obeys the Laplace equation:

$$\frac{\partial^2 \phi}{\partial y^2} + \frac{\partial^2 \phi}{\partial z^2} = 0 \,. \tag{33}$$

The boundary condition at the solid substrate Γ_s is given by the potential of the electrodes:

$$\phi = \pm V \qquad \text{at} \quad y = \mp R_e/2 \,, \tag{34}$$

where R_e is the electrode separation, and the boundary condition at the interface Γ is given by the interfacial jump condition in Eq. (31) in the limit $\epsilon_l \gg \epsilon_g$:

$$E_{n_l} = \frac{\partial \phi}{\partial z} = 0 \,. \tag{35}$$

Equation (33) was solved, subject to the boundary conditions in Eqs. (34) and (35) using the method of images.[10] For simplicity, the solid substrate was shifted downwards to the plane $z = -h$; the interface Γ is then located at $z = 0$. To account for the boundary condition in Eq. (35), two image charges of the same signs as the point electrode charges at $z = -h$ are placed in the plane $z = h$. A combination of the field arising from these four point charges then allows the construction of the Green's function that represents the liquid electrostatic potential. Differentiating this potential with respect to y subsequently gives rise to an expression for the tangential electric field. Evaluating this at the interface $z = 0$ and subsequently expanding in the limit $h/R_e \to 0$ results in the following expression for the tangential liquid field at the interface:[10]

$$E_{t_l} = \frac{4V}{\pi R_e} \left(1 - \frac{8h^2}{R_e^2} \right) \,. \tag{36}$$

As the normal field E_{n_l} vanishes from Eq. (35), the interfacial Maxwell pressure given by Eq. (8) is then dominated by the tangential field in Eq. (36). This tangential liquid electric field is therefore coupled to the hydrodynamics via the film thickness h. Substituting this into Eq. (29) and noting that $h = (x_f - x) \tan \theta_f$, where x_f is
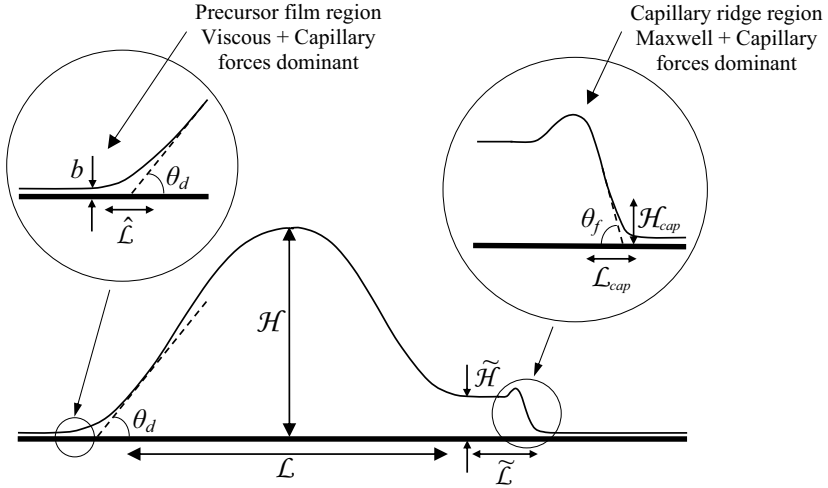
Fig. 5. Spontaneous electrowetting film generated due to the parallel planar line electrode configuration. The insets show enlargements of the precursor film region where viscous and capillary forces are dominant and the capillary ridge region where the Maxwell and capillary forces are dominant. The two regions are characterized by a static contact angle θ_f and an apparent dynamic contact angle θ_d.

the position of the three-phase contact line and θ_f is the contact angle or slope of the capillary ridge (Fig. 5), we obtain

$$p = \gamma \frac{\partial^2 h}{\partial x^2} - \frac{8\epsilon_o \epsilon_l V^2}{\pi^2 R_e^2} \left[1 - \frac{16 \tan^2 \theta_f}{R_e^2} (x_f - x)^2 \right], \tag{37}$$

thus indicating that the tangential field is maximum at the three-phase contact line where $h = 0$, and decays linearly along the interface away from the contact line at $x = x_f$. Unlike the static electrowetting case in Sec. 2.2, the field is not singular at the contact line and the Maxwell pressure gradient arising from the linearly decaying Maxwell stress is macroscopic. It is this macroscopic Maxwell pressure gradient that is responsible for a negative capillary pressure in the contact line region that sucks liquid from the bulk into the vicinity of the tip, thus pushing out a thin spontaneous electrowetting film ahead of the macroscopic spreading drop.

The solid lines depicting the interface height profiles in Fig. 6(a) show the formation of the spontaneous electrowetting film and its propagation ahead of the macroscopic drop. This electrowetting film is absent when there is no electric field present, as shown by the dashed lines in Fig. 6(a), thus suggesting that it is the Maxwell stress, represented by the second term on the right-hand side of Eq. (37) that is responsible for the spontaneous electrowetting film. More specifically, the Maxwell Bond number

$$B = \frac{8\epsilon_o \epsilon_l V^2 \tilde{L}}{\varepsilon \pi^2 \gamma R_e^2} \tag{38}$$

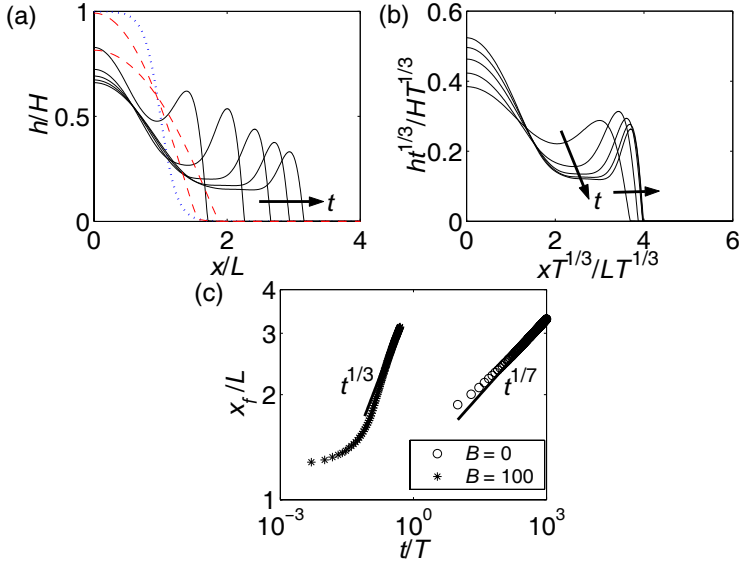has a critical value of 10 below which no electrowetting film is formed.[10]

Fig. 6.   Transient drop and film evolution with Maxwell Bond number $B = 100$. (a) Interface profiles for five equal time steps up to $t/T = 0.5$, where $T = \tilde{L}/U$ is the characteristic time scale; $U = \varepsilon^3 \gamma/\mu$ is the characteristic system velocity. The *dotted line* shows the initial profile at $t/T = 0$ and the *dashed lines* indicate the spreading drop due to pure capillary motion when no electric field is applied ($B = 0$) at $t/T = 1, 10$. (b) Self-similar behavior of the advancing electrowetting film is shown with the collapse of the interface profiles with time by replotting the data in (a) using a similarity transform. (c) Position of the advancing front of the drop radius or the electrowetting film x_f/L with time.

At the three-phase contact line, a dominant force balance is given by the viscous and Maxwell stresses (Fig. 5):

$$\frac{\mu \tilde{U}}{\tilde{H}^2} \sim \frac{p_M}{\tilde{L}}, \tag{39}$$

where $\tilde{H}$ and $\tilde{L}$ are the characteristic height and length scales of the electrowetting film (see Fig. 5), and, $\tilde{U} \sim \tilde{L}/T \equiv \gamma/\mu$ is its characteristic velocity; $p_M = \epsilon_o \epsilon_l E_{t_i}^2/2$ is the Maxwell stress. It is possible to assume, consistent with the numerical results in Yeo and Chang,[10] that the slope of the capillary ridge at the advancing front of the electrowetting film θ_f and the volume per unit width of the electrowetting film

$$V_0 \sim \tilde{H} \tilde{L}, \tag{40}$$

are constant. From Eq. (37), the Maxwell pressure gradient in Eq. (39) for constant θ_f then scales as

$$\frac{\partial p_M}{\partial x} \sim \frac{p_M}{\tilde{L}} \sim \frac{\varepsilon \gamma B \tan^2 \theta_f}{R_e^2}. \tag{41}$$

It then follows from Eqs. (39)–(41) that

$$\tilde{L} \sim \left(\frac{\varepsilon \gamma B \tan^2 \theta_f V_0^2 T}{\mu R_e^2} \right)^{1/3}. \tag{42}$$

Given that θ_f is assumed constant, the Maxwell pressure gradient given by Eq. (41) is constant for a specific electrode separation R_e and hence Eq. (42) rendered dimensionless has the following scaling relation for constant V_0:

$$x \sim t^{1/3}, \tag{43}$$

thus suggesting that the electrowetting film advances in a self-similar manner for Maxwell-dominated spreading. This is confirmed by the results in Fig. 6(b) in which the evolution interfacial height profiles in Fig. 6(a) are rescaled using the similarity scaling in Eq. (43) above; the resulting transformed profiles are shown to collapse in time t. A plot of the position of the electrowetting film advancing front x_f with time also shows that the front progresses as $t^{1/3}$, much faster than the $t^{1/7}$ pure capillary spreading behavior when no electrical stresses are present.

From a detailed similarity analysis of the constant volume electrowetting film, Yeo and Chang[10] have derived a prediction for the position of the advancing film as a function of time:

$$x_f = 0.4 \left[\frac{\epsilon_o \epsilon_l V^2 R_e t}{\mu} \right]^{1/3}, \tag{44}$$

independent of the dimensions and dynamics of the bulk macroscopic drop. In terms of an electrocapillary time scale,

$$T_{\mathrm{cap}} \equiv \frac{\mu L_{\mathrm{cap}}}{\gamma} \equiv \frac{\pi^2 \mu R_e}{8 \epsilon_o \epsilon_l V^2}, \tag{45}$$

where $L_{\mathrm{cap}} \equiv \pi^2 \gamma R_e^2 / 8 \epsilon_o \epsilon_l V^2$ is the electrocapillary length scale (see Fig. 5), Eq. (44) can be expressed as

$$x_f = 0.43 R_e \left(\frac{t}{T_{\mathrm{cap}}} \right)^{1/3}. \tag{46}$$

Figure 7 shows a comparison between the prediction given by Eq. (46) with data from the spontaneous electrowetting experiments of Ahmed *et al.*[28] for deionized water in which plane parallel line electrodes [Fig. 2(d)] were adopted. The close agreement obtained without the need for any empirical fitting parameters thus inspires confidence in the proposed mechanism. We note that the $t^{1/3}$ self-similar Maxwell-dominated spreading is analogous to the self-similar gravity-driven fronts first observed by Huppert.[30] This is because the Maxwell pressure gradient, given by Eq. (41), for a constant capillary ridge slope θ_f, acts as a constant body force term similar to gravity. Akin to gravitational spreading, Maxwell-dominated spreading is not dependent on capillarity or wettability. However, in contrast to gravitational spreading, Maxwell-dominated spreading does not depend on the drop volume — the macroscopic Maxwell pressure is due to interfacial dielectric polarization near the contact line and is hence independent of the drop size.

Yeo and Chang[10] have also derived a dynamic contact angle condition for the bulk macroscopic drop. In the short initial transient before the formation of the
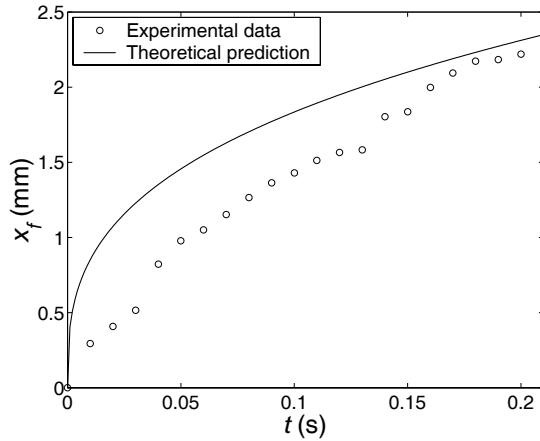
Fig. 7.   Position of the advancing electrowetting film front x_f as a function of time t showing the close agreement between the model prediction (*solid line*) and the experimental data of Ahmed *et al.*[28] for deionized water ($\mu = 1$ cp, $\epsilon_l = 78$, $\epsilon_g = 1$, $V = 200$ V and $R_e = 40$ μm).

spontaneous thin electrowetting, the macroscopic drop spreading dynamics is dominated by pure capillary action driven by molecular wetting. Neglecting the Maxwell stress, the matching region in the vicinity of the three-phase contact line, as shown in Fig. 5, can be described by a dominant balance between the viscous and capillary stresses. In the locally quasi-steady limit with respect to a moving coordinate frame translating at a constant dimensionless speed Ca $\equiv \mu U/\gamma$, where U is the characteristic velocity of the contact line, the spreading dynamics of the drop in the limit $\hat{L}/L \ll 1$ is governed by the Bretherton equation:[31]

$$3\text{Ca}\frac{\partial h}{\partial x} = \frac{\partial}{\partial x}\left(h^3\frac{\partial^3 h}{\partial x^3}\right),$$ (47)

where h is the dimensionless film thickness, scaled by H; the x- and z-coordinates are scaled by the macroscopic drop length scales, L and H, respectively. It can then be shown[10,32,33] that the film height, in dimensional form, has a weak logarithmic asymptotic behavior away from the contact line:

$$h \sim -x\text{Ca}^{1/3}\left(9\log\frac{\hat{L}}{L}\right)^{1/3}.$$ (48)

The dynamic contact angle condition for the spreading macroscopic drop can then be derived as

$$\tan\theta_d \sim -\frac{\partial h}{\partial x} \sim \left(-9\log\frac{\hat{L}}{L}\right)^{1/3}\text{Ca}^{1/3},$$ (49)

where θ_d is the apparent contact angle of the macroscopic drop. $\hat{L}/L \ll 1$ is a dimensionless molecular length scale, equivalent to the molecular precursor film

thickness,

$$\frac{\hat{L}}{L} \sim \frac{b}{H}, \tag{50}$$

the Hamaker constant,

$$\frac{\hat{L}}{L} \sim \frac{1}{L}\sqrt{\frac{|\alpha|}{6\pi\gamma}}, \tag{51}$$

or the slip coefficient,

$$\frac{\hat{L}}{L} \sim \lambda_i^{1/(1+i)}, \tag{52}$$

depending on the mechanism (molecular precursor film, disjoining pressure or slip condition) adopted to remove the contact line singularity in perfectly or partially wetting fluids.[10] In the above, b is the molecular precursor film thickness, α the Hamaker constant and $\lambda_i = \lambda h^i$ $(i = 0, 1)$ the slip coefficient; λ is the film thickness dependent slip length, the dependence for which is given by the exponent i and corresponds to the different slip models historically used.[34] We note, however, that the $x \log x$ behavior suggests that the macroscopic drop spreading dynamics is universal and independent of the intermolecular interactions at the contact line that give rise to slip or a microscopic molecular precursor film to leading order. Equation (49) also shows that local quasi-steady spreading of a perfectly or partially wetting fluid at constant speed Ca driven by viscous and capillary forces always gives rise to a interfacial shape with a slope that scales as $Ca^{1/3}$, in accordance to Tanner's law.[35] Thus, for spontaneous electrowetting films the static change in the macroscopic contact angle given by the Lippmann condition in Eq. (6) is no longer relevant. Instead, the front of the advancing electrowetting film can be characterized by a constant capillary ridge slope θ_f and an apparent dynamic macroscopic contact angle θ_d, the latter defined by Eq. (49) from a dominant balance between viscous and capillary stresses at the three-phase contact line region.

4. Conclusion

The manipulation of drops and films using electric fields exhibits rich and varied behavior depending on the nature and geometry of the system. As a result, there have often been some overlap and confusion in the literature with regards to the terminology used or the mechanisms ascribed to various observations. We have therefore sought to clarify the different phenomena by re-emphasizing and delineating the classical physical laws that govern electrocapillary phenomena and electrowetting. In addition, we have also sought to distinguish static electrowetting from spontaneous electrowetting. The latter occurs when a bulk Maxwell pressure gradient exists to drive a flow towards the contact line. While bulk forces can only be balanced by viscous dissipation due to a bulk flow, microscopic forces localized at the contact line can be cancelled by opposing surface forces. This occurs for the

Table 1.　Comparisons between static and spontaneous electrowetting.

Static Electrowetting	Spontaneous Electrowetting
Dielectric film-coated plate electrodes	Planar parallel line electrodes
Normal vapor phase electric field	Tangential liquid phase electric field
Singular electric field • Confined to small region $\sim d$	Non-singular electric field • Vanishes when $h \sim R_e$
Localized Maxwell pressure gradient • Point force at contact line • Balances surface forces (no net force) • No flow into contact line region	Macroscopic Maxwell pressure gradient • Constant body force in contact line region • No balance with surface forces • Macroscopic bulk flow into contact line region
No spontaneous electrowetting film • Static change in macroscopic contact angle • Consistent with Lippmann condition	Spontaneous electrowetting film • Analogous to self-similar gravity spreading • Constant electrowetting film capillary ridge slope

former electrowetting phenomenon, where a static contact angle dependence on the field arises.

The main distinctions between static and spontaneous electrowetting are summarized in Table 1. In particular, the weakly singular vapor phase electric field that arises when dielectric film-coated planar plate electrodes are used, blow up within a confined region which has a length scale of the same order as the dielectric film thickness d. The Maxwell pressure gradient that arises is therefore localized and microscopic. Integrating the microscopic Maxwell pressure gives rise to a point force at the contact line, which balances the surface forces exactly such that there is no net force and hence no bulk liquid motion. As a result, only a static change in the macroscopic contact angle arises due to the Maxwell pressure, as described by the Lippmann condition; no spontaneous electrowetting films occur in this case. On the other hand, if planar parallel line electrodes are employed, the resultant tangential liquid electric field at the contact line is not singular and decays linearly away from the contact line along the interface. The Maxwell pressure gradient that arises is therefore macroscopic and extends into the bulk region. The bulk forces can no longer be balanced by the surface forces at the contact line and bulk liquid motion is induced by the negative capillary pressure, thus pushing out a thin spontaneous electrowetting film that advances much faster than the macroscopic drop. For an electrowetting film with constant volume and constant capillary ridge slope, we show that the front of this electrowetting film advances in a self-similar manner as $t^{1/3}$, analogous to gravity spreading films.

Acknowledgments

References

1. G. Lippmann, *Ann. Chim. Phys.* **5** (1875) 494.
2. M. W. J. Prins, W. J. J. Welters and J. W. Weekamp, *Science* **291** (2001) 277.
3. J. O'M. Bockris and A. K. N. Reddy, *Modern Electrochemistry* (Plenum, New York, 1970).
4. G. Beni and S. Hackwood, *Appl. Phys. Lett.* **38** (1981) 207.
5. J. Lee and C.-J. Kim, *J. Microelectromech. Syst.* **9** (2000) 171.
6. T. B. Jones, *Langmuir* **18** (2002) 4437.
7. H. A. Pohl, *J. Appl. Phys.* **22** (1951) 869.
8. H. A. Pohl, *Dielectrophoresis* (Cambridge University, Cambridge, 1978).
9. D. A. Saville, *Ann. Rev. Fluid Mech.* **29** (1997) 29.
10. L. Y. Yeo and H.-C. Chang, submitted to *Phys. Rev.* **E**.
11. M. Schneemilch, W. J. J. Welters, R. A. Hayes and J. Ralston, *Langmuir* **16** (2000) 2924.
12. T. D. Blake, A. Clarke and E. H. Stattersfield, *Langmuir* **16** (2000) 2928.
13. B. Janocha, H. Bauser, C. Oehr, H. Brunner and W. Göpel, *Langmuir* **16** (2000) 3349.
14. C. Decamps and J. De Coninck, *Langmuir* **16** (2000) 10150.
15. M. Vallet, M. Vallade and B. Berge, *Eur. Phys. J.* **B11** (1999) 583.
16. P. W. Chudleigh, *Appl. Phys. Lett.* **21** (1972) 547.
17. A. Quinn, R. Sedev and J. Ralston, *J. Phys. Chem.* **B107** (2003) 1163.
18. R. Digilov, *Langmuir* **16** (2000) 6719.
19. C. Quillet and B. Berge, *Curr. Opin. Colloid Interface Sci.* **6** (2001) 34.
20. M. J. de Ruijter, T. D. Blake and J. De Coninck, *Langmuir* **15** (1999) 7836.
21. T. Chou, *Phys. Rev. Lett.* **87** (2001) 106101.
22. J. Buehrle, S. Herminghaus and F. Mugele, *Phys. Rev. Lett.* **91** (2003) 086101.
23. C. Huh and L. E. Scriven, *J. Colloid Interface Sci.* **35** (1971) 85.
24. V. E. B. Dussan and S. H. Davis, *J. Fluid Mech.* **65** (1974) 71.
25. K. H. Kang, *Langmuir* **18** (2002) 10318.
26. L. G. Leal, *Laminar Flow and Convective Transport Processes* (Butterworth-Heinemann, Newton, MA, 1992).
27. T. B. Jones, M. Gunji, M. Washizu and M. J. Feldman, *J. Appl. Phys.* **89** (2001) 1441.
28. R. Ahmed, D. Hsu, C. Bailey and T. B. Jones, *Proc. Int. Conf. Microchannels and Minichannels*, ICMM2003–1110 (Rochester, NY, 2003).
29. D. Ausserré, A. M. Picard and L. Léger, *Phys. Rev. Lett.* **57** (1986) 2671.
30. E. Huppert, *Nature* **300** (1982) 427.
31. F. P. Bretherton, *J. Fluid Mech.* **10** (1961) 166.
32. S. Kalliadasis and H.-C. Chang, *Phys. Fluids* **6** (1994) 12.
33. S. Kalliadasis and H.-C. Chang, *Ind. Eng. Chem. Res.* **35** (1996) 2860.
34. P. J. Haley and M. J. Miksis, *J. Fluid Mech.* **223** (1991) 57.
35. L. H. Tanner, *J. Phys.* **D12** (1979) 1473.